Ultrafast Electron Transfer Dynamics in Ruthenium Polypyridyl Complexes with a π-Conjugated Ligand†

Joseph D. Henrich,‡ Haoyu Zhang,‡ Prabir K. Dutta,‡ and Bern Kohler*,§

Department of Chemistry, The Ohio State University, 120 West 18th Avenue, Columbus, Ohio 43210, and Department of Chemistry and Biochemistry, Montana State University, P.O. Box 173400, Bozeman, Montana 59717

Received: March 28, 2010; Revised Manuscript Received: June 16, 2010

The excited-state dynamics of two mixed-ligand mononuclear ruthenium(II) complexes, $[(bpy)_2RuL_{DQ}]^{4+}$ (where bpy = 2,2′-bipyridine, L_{DQ} = 1-[4-(4′-methyl)-2,2′-bipyridyl)]-2-[4-(4′-*N*,*N*′-tetramethylene-2,2′-bipyridinium]) and $[(bpy)_2RuL]^{2+}$ (where L = 1, 2-bis[4-(4′-methyl)-2,2′-bipyridyl)]ethene), were investigated by femtosecond transient absorption spectroscopy. Photoexcitation of the $[(bpy)_2RuL_{DQ}]^{4+}$ complex at three separate pump wavelengths leads to a common charge-separated state consisting of Ru^{3+} and an excited electron delocalized over the extended π-system centered on the ethenyl moiety of the L_{DQ} ligand. In $[(bpy)_2RuL]^{2+}$, the excited electron is unable to delocalize throughout the π system and remains on the bipyridyl end of ligand L closest to the ruthenium atom. Vibrational cooling in the charge-separated state of $[(bpy)_2RuL_{DQ}]^{4+}$ indicates that this state is formed faster than excess energy can be dispersed to the solvent and orders of magnitude more rapidly than in previously studied ruthenium-diquat or ruthenium-viologen dyads with nonconjugated linkers.

1. Introduction

A long-standing goal of solar energy research is the development of chemical systems that use sunlight to generate charge-separated (CS) states by photoinduced electron transfer (ET).[1] Photoexcitation of a covalently linked donor−acceptor complex or dyad can create a CS state via intramolecular ET, and the underlying events are highly amenable to study by time-resolved laser spectroscopy. The CS state formed by forward ET should be produced with a high quantum yield and be sufficiently long-lived for follow-on reactions to make use of its stored energy. Dyad compounds consisting of a ruthenium(II) polypyridyl photosensitizer with covalently attached bipyridinium electron acceptors have shown promise in the past,[2−4] but efforts to accelerate the rate of forward ET have often resulted in an undesirable increase in the rate of back ET.[4−6]

Many investigators have used ultrafast laser spectroscopy to study the photophysics of transition metal polypyridyl complexes.[6−17] Complexes with elongated ligands that position the ruthenium core farther away from the eventual charge acceptor have been studied as a strategy for slowing the charge recombination that quenches the CS state.[3−6,18−20] Increasing this distance slows charge recombination but has the undesirable side effect of decreasing the rate of forward ET so greatly that it frequently falls below the rate of back ET, resulting in insignificant population of the CS state.[20]

Although there have been many studies of ruthenium polypyridyl complexes covalently tethered to electron acceptors via saturated bridges,[3,4,20−22] there have been fewer investigations of ruthenium-based dyads with π-conjugated bridges.[23−25] Nevertheless, there is growing interest in the role that a π-conjugated bridge separating donor and acceptor moieties plays in mediating forward and back ET.[26−29] So-called molecular wires attached to photoactive transition metal cores provide effective pathways for rapidly transmitting electrons over substantial distances.[29]

CHART 1

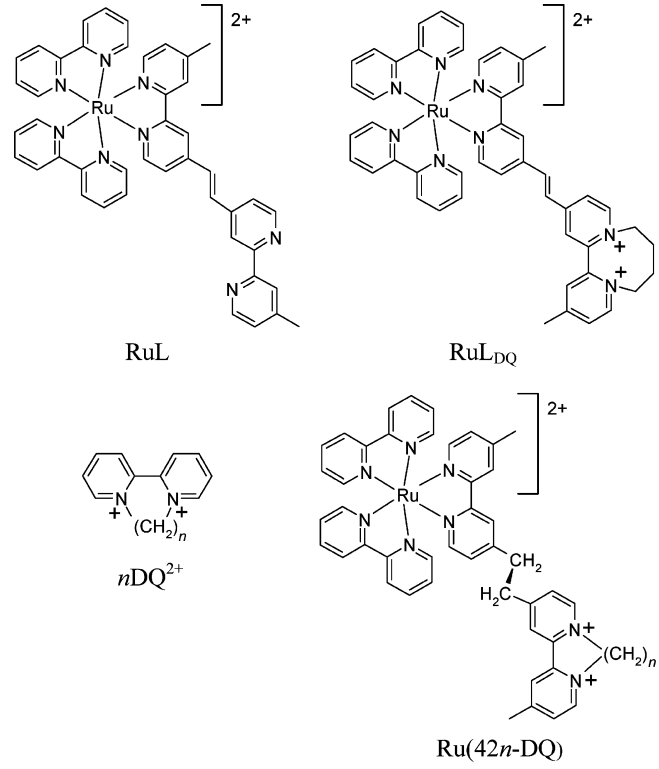

To better understand how a conjugated bridge affects rates of intramolecular ET in ruthenium polypyridyl complexes, we have studied the mixed-ligand ruthenium photosensitizer $[(bpy)_2RuL_{DQ}]^{4+}$ (Chart 1) by broadband femtosecond transient absorption spectroscopy in acetonitrile solution. Here, bpy is 2,2′-bipyridine and ligand L_{DQ} is (1-[4-(4′-methyl)-2,2′-bipyridyl]-2-[4-(4′-*N*,*N*′-tetramethylene-2,2′-bipyridinium)]ethene), a quater-

† Part of the "Michael R. Wasielewski Festschrift".

* To whom correspondence should be addressed. E-mail: kohler@chemistry.montana.edu.

‡ The Ohio State University.

§ Montana State University.

10.1021/jp102776r
Published on Web 07/15/2010

nized version of ligand L (1,2-bis(4-(4′-methyl)-2,2′-bipyridyl)ethene). The nonquaternized $[(bpy)_2RuL]^{2+}$ (Chart 1) was also studied. Hereafter, we will refer to $[(bpy)_2RuL_{DQ}]^{4+}$ as RuL_{DQ} and $[(bpy)_2RuL]^{2+}$ as RuL.

Compound RuL_{DQ} was developed as a photosensitizer that can be attached to the surface of a zeolite particle by ship-in-a-bottle quaternization of the terminal 2,2′ bipyridyl group of ligand L in RuL.[30,31] The size of L prevents the ruthenium core from moving on the surface.[30] Restricting ligand conformational mobility in ruthenium−viologen dyads is one strategy for slowing down charge recombination.[32] A further attractive but unexplored aspect of this ligand is its π-conjugation, which could accelerate electron transport from the metal center to the terminal diquat acceptor.

Zhang et al.[31] recently studied the charge transfer reaction between RuL_{DQ} anchored in a zeolite supercage and methyl viologen molecules ion-exchanged into the zeolite. Using nanosecond laser instrumentation, these authors were unable to detect any transient emission, suggesting that rapid excited state deactivation takes place. They observed further that RuL is emissive, whereas emission by RuL_{DQ} is nearly completely quenched.[31] They proposed that in RuL_{DQ}, fast intramolecular charge transfer quenches the long-lived ^{3}MLCT excited state usually seen in ruthenium(II) photosensitizers.[31] These findings highlight the need for better characterization of the photophysics of RuL_{DQ} and were a further motivation for this study.

2. Experimental Section

Samples. RuL and RuL_{DQ} were synthesized as described previously.[31,33] Salts with PF_6^- counterions were prepared because of their good solubility in acetonitrile. Acetonitrile was obtained from Burdick and Jackson and used as received. Steady-state absorption spectra were recorded using a Perkin-Elmer Lambda 25 UV/vis spectrophotometer. Solutions were held in a 1 mm path length fused-silica cuvette.

Transient Absorption Measurements. Broadband transient absorption spectra and kinetic experiments at a single probe wavelength were recorded using a femtosecond pump−probe spectrometer described elsewhere.[34] Briefly, a Ti:Sapphire oscillator and regenerative amplifier (Coherent Inc.) produced 50 fs pulses at 800 nm with a repetition rate of 1 kHz. A portion of this output was split off and used to pump optical parametric amplifiers for generating excitation wavelengths at 320, 400, 540, and 600 nm. A second portion was split off for white light generation and used as the probe and reference in a broadband transient absorption setup. A motorized linear optical delay stage with a maximum time delay of 3.5 ns was used to delay the probe pulse relative to the pump pulse. An 800 nm pulse was focused onto a 1 mm CaF_2 plate to generate a white light continuum. The CaF_2 plate was rotated 1.5° every 3 s to improve the long-time stability of the continuum. A 50 mm lens collimated the continuum light, which was subsequently passed through an iris to select a uniform region. The continuum was split into probe and reference beams using reflections from the front (probe) and back (reference) surfaces of a 6-mm-thick CaF_2 plate. The reference beam passed through the sample 3 mm away from the position of the overlapped pump and probe beams. The pump beam was blocked after the sample and the probe, and reference beams were focused onto the entrance slit (0.5 mm) of a Triax 550 polychromator (Jobin Yvon) and detected using a thermoelectrically cooled Symphony CCD camera (Jobin Yvon). The pump and probe beams were linearly polarized, and the angle between their planes of polarization was set to the magic angle (54.7°) for all experiments performed in this study to remove reorientational dynamics.

CCD camera image acquisition was referenced to an optical chopper (New Focus model 3501) positioned in the probe beam (50% blocked/50% open, 25 Hz), which allowed every other group of 20 probe pulses to reach the detector. A chopper in the pump path (75% blocked/25% open, 12.5 Hz) allowed 20 pump pulses to reach the sample, coinciding with every other set of probe pulses. Probe spectra were recorded in this manner in the presence and absence of the pump. This process was repeated 250 times at each delay point. The difference between pump on and pump off spectra was used to calculate the difference absorption spectrum. The instrument response was ~250 fs. Solutions were flowed to avoid re-excitation of the sample using a flow cell with CaF_2 windows and a 1 mm path length. RuL and RuL_{DQ} solutions for transient absorption experiments were prepared to have a ground state absorbance of about 0.3 at 400 nm, corresponding to a solute concentration of ~0.5 mM.

Spectroelectrochemistry. Spectroelectrochemical measurements were conducted in an optically transparent thin-layer electrochemical (OTTLE) cell (CH Instruments). The 1 mm path length cell is equipped with a Pt gauze working electrode, a Pt wire counter electrode, and a Ag/AgCl reference electrode. Spectra were recorded with a UV-2501PC spectrophotometer (Shimadzu). Solutions were prepared immediately before addition to the cell and were purged with N_2 for 15 min before use. Absorption spectra of the reduced species were recorded between 250 and 800 nm after drawing new solution into the OTTLE cell, applying the desired potential to the Pt minigrid electrode, and waiting until minimal current was being passed, usually after 1 to 5 min. Samples were prepared with 0.1 M tetrabutylammonium hexafluorophosphate as a supporting electrolyte.

Global Fitting Analysis. Decay transients (ΔA vs delay time) were analyzed by global nonlinear least-squares fitting. Broadband transient absorption difference spectra, $\Delta A(t, \lambda_{pr})$, depend explicitly on delay time, t, between pump and probe pulses and on the probe wavelength, λ_{pr}. Transient spectra were recorded at nonequally spaced delay times. To reduce the quantity of data for analysis, spectra at each delay time were sampled every 5 nm. Each two-dimensional data set was analyzed by global fitting to a sum of n exponentials using eq 1,

$$\Delta A(t, \lambda_{pr}) = \sum_{i=1}^{n} D_i(\lambda_{pr}) \cdot \exp(-t/\tau_i) \otimes \mathrm{IRF}(t) \qquad (1)$$

In this equation, the τ_i are exponential time constants which were globally linked for kinetic signals at all probe wavelengths

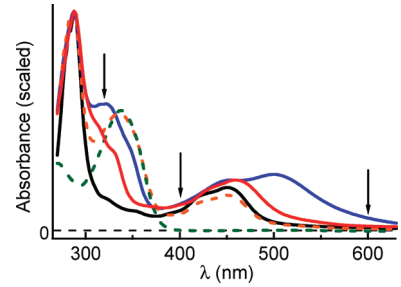

Figure 1. Normalized absorption spectra in acetonitrile solution of $[Ru(bpy)_3]^{2+}$ (black), L_{DQ} (dashed green), 1:1 molar mixture of $[Ru(bpy)_3]^{2+}$ and L_{DQ} (dashed orange), RuL (red), and RuL_{DQ} (blue). Arrows indicate excitation wavelengths used in transient absorption measurements: 320, 400, and 600 nm.

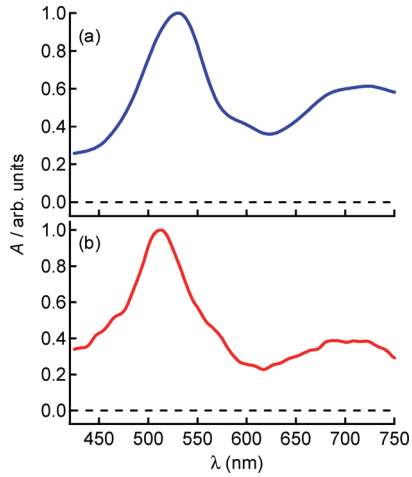

Figure 2. Absorption spectra of (a) one-electron-reduced ligand L_{DQ} and (b) one-electron-reduced ligand L, each generated electrochemically.

in a given data set; $D_i(\lambda_{pr})$ are probe-wavelength-dependent amplitudes that define the decay-associated difference spectrum (DADS)[35] associated with each decay component, τ_i; and $\otimes IRF(t)$ represents convolution with a Gaussian of fwhm 250 fs that represents the finite instrument response. The DADS were then used to estimate spectra of the various transient species, as will be described more fully in section 3.3.

3. Results

3.1. Steady-State Spectroscopy. UV/vis absorption spectra measured in acetonitrile solution for RuL, RuL_{DQ}, $[Ru(bpy)_3]^{2+}$, and bare ligand L_{DQ} are shown in Figure 1. There is good agreement with previously published spectra of RuL,[33] $[Ru(bpy)_3]^{2+}$,[7] and RuL_{DQ}.[31] The RuL and RuL_{DQ} spectra are similar below 450 nm. Each exhibits a band at 287 nm and another band at ~330 nm, which is more intense for L_{DQ}. The isolated L_{DQ} ligand has transitions at 287 and 336 nm but does not absorb at visible wavelengths. Both RuL and RuL_{DQ} have ^{1}MLCT transitions near 460 nm. RuL_{DQ} exhibits an even longer wavelength absorption band near 500 nm.

To facilitate assignment of the transient spectra, steady-state spectra of reduced ligands L and L_{DQ} were recorded, following electrochemical reduction in an OTTLE cell. A potential of −1.8 V vs Fc^+/Fc was used for ligand L and −0.4 V vs Fc^+/Fc for L_{DQ}. The reduced L_{DQ} ligand shows two prominent peaks at 525 and 720 nm (Figure 2a). The reduced L ligand shows absorption maxima at 510 and 700 nm (Figure 2b) and agrees reasonably well with a previously reported spectrum.[18]

3.2. Femtosecond Pump−probe Measurements. *RuL_{DQ}*. Broadband transient spectra were recorded for RuL_{DQ} in acetonitrile at pump wavelengths of 320, 400, and 600 nm. Representative spectra at each pump wavelength are shown in Figure 3 in three delay time windows. At delay times >100 ps (right column, Figure 3), identical spectra and spectral evolution are seen at all pump wavelengths within experimental uncertainty. At delay times of <100 ps (left and center columns in Figure 3), subtle yet reproducible differences with excitation wavelength are visible. The data sets obtained with pump wavelengths of 322 and 400 nm require three exponentials for fitting. On the other hand, there is little improvement in the quality of the fit to the 600 nm pump data when using three versus two exponentials, and this data was therefore analyzed

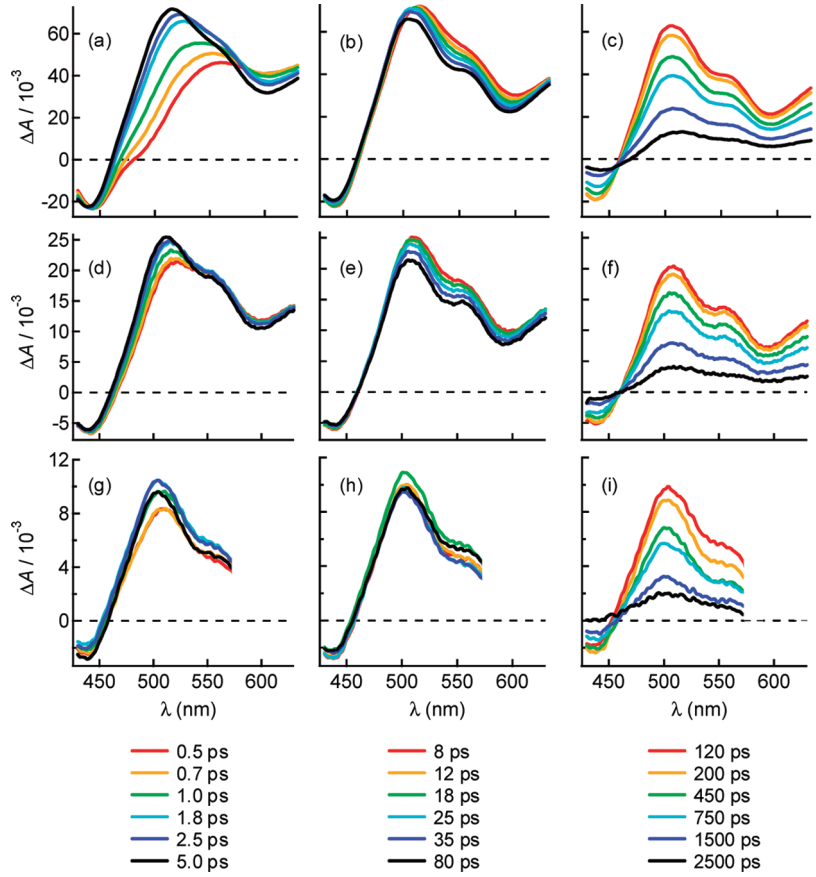

Figure 3. Transient spectra of RuL_{DQ} in acetonitrile following excitation at 320 nm (panels a−c), 400 nm (panels d−f), and 600 nm (panels g−i) at the delay times given below each column of panels.

TABLE 1: Best-Fit Lifetimes (ps) for RuL_{DQ}[a]

solvent	λ_{pump} (nm)	τ_1	τ_2	τ_3
CH_3CN	320	1.2 (0.08)	11.7 (2.1)	1430 (60)
	400	1.03 (0.08)	16 (5)	1460 (70)
	600	0.56 (0.1)		1270 (61)

[a] Uncertainties in parentheses are twice the estimated standard error.

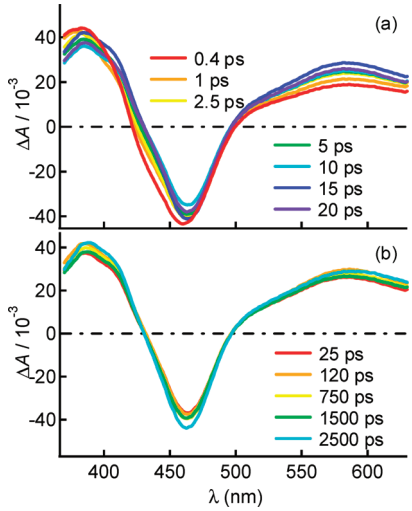

Figure 4. Transient spectra of RuL in acetonitrile following excitation at 320 nm at delay times between (a) 0.4 and 20 ps, and (b) 25 and 2500 ps.

with just two decay components. All exponential lifetimes are summarized in Table 1. The shortest time constant (τ_1) decreases as the pump wavelength is increased. During the τ_1 decay (leftmost column of Figure 3), a bleach band is evident at 440 nm together with a more intense positive band between 480 and 560 nm. The latter band grows in amplitude, and its maximum shifts to shorter wavelengths during the first few picoseconds after the pump pulse. The growth and shifting diminish at longer excitation wavelengths, and at 600 nm, only modest amplitude changes are seen with little indication of blue shifting.

For excitation at 320 nm, the positive spectral bands during the τ_2 decay shift by 10−20 nm to shorter wavelengths (Figure 3b). A somewhat smaller shift is still visible for excitation at 400 nm (Figure 3e), but none is evident for a pump wavelength of 600 nm (Figure 3h). This is the reason why the intermediate decay time (τ_2) is absent in the 600 nm data set. Despite pump wavelength-induced differences in the spectral dynamics at earliest times (compares Figure 3a, d, and g), identical signals are observed at delay times >100 ps (rightmost column in Figure 3), regardless of excitation wavelength.

For RuL_{DQ} in acetonitrile, excitation at 320 nm yields a spectrum that is most intense near 550 nm at earliest delay times and which rapidly evolves ($\tau_1 \approx 1$ ps) to one with λ_{max} of 500 nm. For excitation at 400 nm, there is again a rapid blue shifting of the transient spectrum at the earliest delay times, but the magnitude of the spectral shift is less pronounced. For all pump wavelengths, virtually no changes on the picosecond time scale are seen at probe wavelengths >600 nm.

Attempts to detect time-resolved emission signals from RuL_{DQ} in acetonitrile using a time-correlated, single-photon counting apparatus with 30 ps time resolution were unsuccessful. No emission was observed between 600 and 700 nm using excitation pulses at 295 nm.

RuL. A broad positive band is seen in the difference spectrum between 500 and 650 nm with a maximum at 580 nm, and strong bleaching is seen at 460 nm when RuL is excited by a 320 nm pump pulse (Figure 4). Spectral amplitudes change modestly at short delay times, but after 20 ps, the transient spectrum remains constant out to the longest delay time studied (2.5 ns). With this short delay time range, it was impossible to monitor the evolution of the excited state of RuL, which has an emission lifetime of hundreds of nanoseconds.[33] Global nonlinear least-squares fitting to two exponentials plus a constant offset gave time constants of 0.14 and 2.6 ps (Table 2). The RuL transient absorption spectrum in Figure 4b is similar to the spectrum reported by Strouse et al.[18] for the related complex $[(dmb)_2Ru(L)]^{2+}$ (dmb = 4,4′-dimethyl-2,2′-bipyridine) 80 ns after 460 nm excitation.

TABLE 2: Best-Fit Lifetimes (ps, unless otherwise noted) for RuL[a]

solvent	λ_{pump} (nm)	τ_1	τ_2	τ_3
CH_3CN	450[b]		256 ns[b]	710 ns[b]
	320	0.14 (0.04)	2.6 (0.2)	∞

[a] Uncertainties in parentheses are twice the estimated standard error. [b] Ref 33.

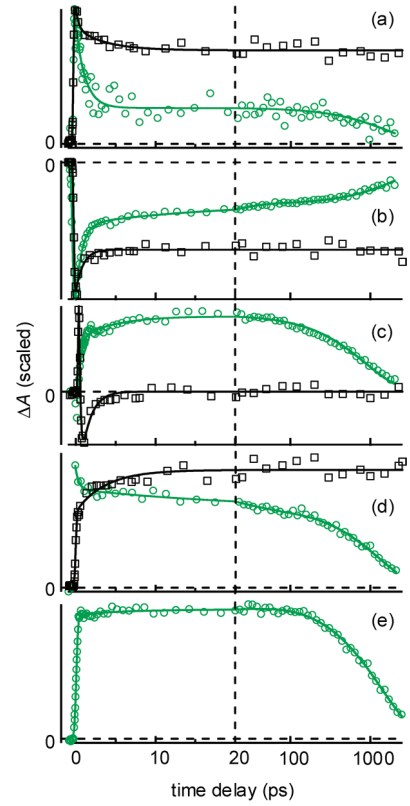

Figure 5. Transient absorption vs time for RuL (black squares) and RuL_{DQ} (green circles) probed at (a) 375, (b) 450, (c) 500, (d) 600, and (e) 740 nm. The pump wavelength was 320 nm for panels a−d and 540 nm for panel e. The time delay axis switches from linear to logarithmic at 20 ps. Fits to the data are shown by solid curves.

Single-Wavelength Kinetics. Figure 5 shows transient absorption traces at selected probe wavelengths between 375 and 740 nm for RuL and RuL_{DQ}. The decay at 375 nm is of lower amplitude for RuL than for RuL_{DQ}. The same trend is seen for the bleach signals at 450 nm. Finally, the signal at 500 nm for RuL is very close to zero after complex dynamics during the initial 5 ps. Kinetic traces recorded for RuL_{DQ} at a pump wavelength of 600 nm were similar to ones recorded at the shorter two pump wavelengths except that the τ_2 component was absent.

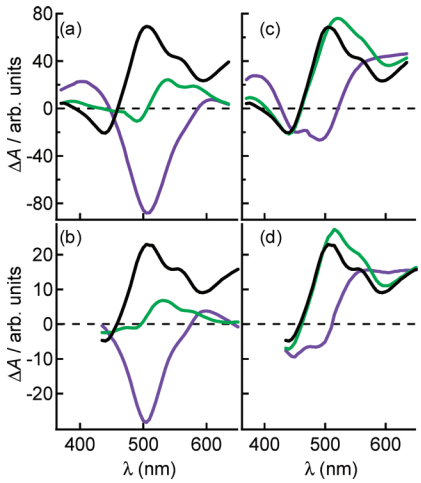

Figure 6. Decay-associated difference spectra for RuL_{DQ} in acetonitrile for excitation at (a) 320 and (b) 400 nm: τ_1 (purple), τ_2 (green), and τ_3 (black). Species associated difference spectra formed from linear combinations of the DADS for excitation at (c) 320 and (d) 400 nm: states A (purple), B (green), and C (black); see Scheme 1.

3.3. Kinetic Modeling and Target Analysis. Transient absorption spectroscopy is a form of difference spectroscopy in which the signal is given by a sum of difference spectra between each transient species present at delay time t and the ground state absorption spectrum. DADS (see section 2) for RuL_{DQ} are shown in Figure 6a and b for pump wavelengths of 320 and 400 nm, respectively. DADS do not correspond generally to difference spectra of actual transient species. Instead, species-associated difference spectra (SADS) are calculated from linear combinations of DADS.[35,36] The needed linear combinations are determined by solving the differential equations of a postulated kinetic model for the species concentrations as a function of time. Here, we made the simple but common assumption of a sequential kinetic model,

$$G \xrightarrow{h\nu_{pump}} A \xrightarrow{k_1} B \xrightarrow{k_2} C \xrightarrow{k_3} G \qquad \text{(Scheme 1)}$$

where k_1, k_2, and k_3 are the first-order rate constants determined from global fitting ($k_1 = \tau_1^{-1}$ etc.), A, B, and C represent transient excited states, and G stands for the electronic ground state. The appropriateness of this model will be discussed in section 4. SADS were calculated for each transient state using the following equations,

$$\text{SADS(A)} = \text{DADS}(k_1) + \text{DADS}(k_2) + \text{DADS}(k_3) \tag{2}$$

$$\text{SADS(B)} = \frac{k_1 - k_2}{k_1}\text{DADS}(k_2) + \frac{k_1 - k_3}{k_1}\text{DADS}(k_3) \tag{3}$$

$$\text{SADS(C)} = \frac{(k_1 - k_3)(k_2 - k_3)}{k_1 k_2}\text{DADS}(k_3) \tag{4}$$

and results are shown in Figure 6c and d for the two pump wavelengths.

SADS(A) for RuL_{DQ} excited at 320 nm (purple curve in Figure 6c) shows positive absorption at 400 and >550 nm with a double-welled bleach between. The bleach minima at 450 and 500 nm match the positions of the ^{1}MLCT transitions in the UV/vis spectrum of RuL_{DQ} (blue curve, Figure 1). SADS(B) and SADS(C) are very similar to each other, but the former is broadened and extends to longer wavelengths as compared with the latter. Overall, similar SADS are observed at both pump wavelengths.

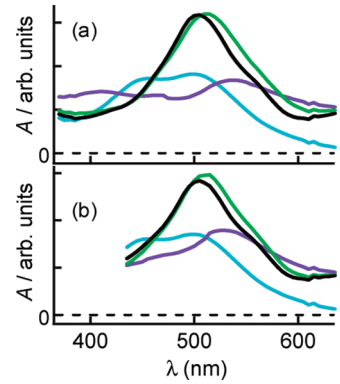

Figure 7. Species associated spectra for RuL_{DQ} excited at (a) 320 nm and (b) 400 nm obtained by adding the scaled ground state absorption spectrum (cyan curve) to the species associated difference spectra in Figures 6c and d: state A (purple), B (green), and C (black).

To obtain species associated spectra (SAS), it is necessary to add the ground state absorption spectrum to each SADS multiplied by a scaling factor, which is generally unknown. Because there is strong ground state absorption in the spectral window (approximately 350−650 nm) of this study, the SAS differ significantly in appearance from their associated SADS. Figure 7 shows the SAS for RuL_{DQ} transient species A, B, and C for excitation at 320 and 400 nm. The cyan curve in Figure 7 shows the scaled ground state absorption spectrum that was added to the SADS in Figure 6c and d to generate the SAS shown in Figure 7. The scaling of the ground state absorption spectrum was chosen to make the SAS everywhere positive and to give reasonably smoothly varying band shapes. The precise scaling is somewhat arbitrary, but it is justified by the good agreement with the spectrum of the reduced ligand (see below). Importantly, the finding that the spectrum of state C has a maximum near 500 nm is insensitive to the precise scaling. Figure 8 shows estimated DADS, SADS, and SAS for RuL estimated with the sequential kinetic model in Scheme 1.

4. Discussion

4.1. Ground State Absorption Spectra. The strong 290 nm absorption band visible in the steady-state absorption spectra of RuL and RuL_{DQ} (Figure 1) is from a bpy ligand-centered $^1\pi \rightarrow \pi^*$ transition and is seen in the spectra of many ruthenium polypyridyl complexes, including $[Ru(bpy)_3]^{2+}$.[37] Absorption between 300 and 350 nm by RuL and RuL_{DQ} (Figure 1) is mostly due to $^1\pi \rightarrow \pi^*$ transitions localized on ligands L and L_{DQ}, respectively. Absorption at wavelengths >400 nm is due to metal-to-ligand charge transfer (MLCT) absorption.[37] The ^{1}MLCT band of RuL is red-shifted by approximately 10 nm to longer wavelengths compared to the ^{1}MLCT band of $[Ru(bpy)_3]^{2+}$. A red-shift of similar magnitude was observed previously for the $(dmb)_2RuL$ complex studied by Strouse et al.[18]

The ^{1}MLCT band of RuL_{DQ} is shifted much farther to the red with λ_{max} of ~500 nm in acetonitrile solution (Figure 1). The appearance of this new band reveals significant electronic interaction between the ruthenium core and the L_{DQ} ligand and indicates that the lowest energy ^{1}MLCT transition is associated

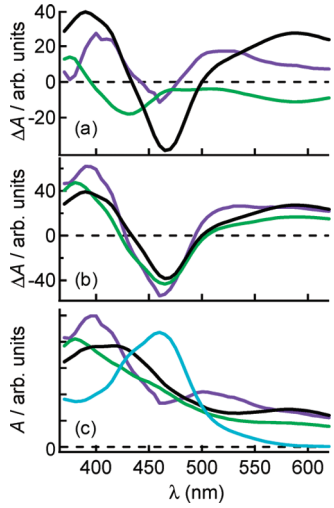

Figure 8. Target analysis of transient spectra for RuL in acetonitrile pumped at 320 nm: (a) DADS, (b) SADS, and (c) SAS. All curves are colored as in Figures 6 and 7.

with the functionalized ligand. Ruthenium polypyridyl complexes having ligands with strongly delocalized π systems frequently show strongly red-shifted MLCT absorption.[38] For example, similar red shifts in MLCT absorption bands of bi- and trinuclear ruthenium complexes linked by conjugated ditopic ligands were reported by Benniston et al.[39] In addition, N-methylation of pendant pyridyl groups of terpyridine ligands red-shifts the MLCT absorption bands of their ruthenium complexes,[40] when the resulting pyridinium groups are directly attached to the metal-ligating bipyridine. In contrast, the absorption spectra of ruthenium polypyridyl complexes linked to bipyridinium acceptors by saturated bridges typically differ minimally from the sum of the individual spectra,[4,5,20] consistent with weak coupling.

Ruthenium polypyridyl complexes that lack new absorption features despite the presence of a π-conjugated bridge are known. For example, coordinating napthalenediimide to ruthenium via a *p*-phenylene spacer produces negligible changes as compared with $[Ru(bpy)_3]^{2+}$.[32] Kim et al. studied the related complexes RuL′ (L′ = 1,4-bis[2-(4′-methyl-2,2′-bipyrid-4-yl)ethenyl]benzene) and its quaternized analog RuL'_{DQ}.[41] These compounds differ from RuL and RuL_{DQ} by the insertion of a *p*-phenylene vinylene unit between the ethenyl group and the ligand terminus. There is little difference between the MLCT absorption of RuL′ and RuL'_{DQ}, but absorption by each is red-shifted by 10 nm as compared with $[Ru(bpy)_3]^{2+}$.[41] Compared with RuL_{DQ}, the above complexes may have attenuated coupling as a result of the greater length of their π-conjugated bridges or because of out-of-plane twisting by the phenylene spacers.

4.2. Long-Lived Excited States in RuL and RuL_{DQ}. Adding a tetramethylene bridge between the nitrogens of the distant bipyridine group of ligand L changes complex RuL into RuL_{DQ} and drastically alters its excited-state dynamics. This bridge forms a pair of quaternary nitrogens or "diquat", which completely quenches the RuL emission.[31] Emission from RuL occurs out to microseconds, but no emission is seen from RuL_{DQ} in steady-state experiments[31] or by TCSPC measurements with a time resolution of 30 ps.

Despite differences in the short-time dynamics, which will be analyzed in more detail later, excitation of RuL_{DQ} at 322, 400, and 600 nm yields the same final state difference spectrum (compare panels c, f, and i in Figure 3). In contrast, a very different transient absorption difference spectrum is observed

TABLE 3: Reduction Potentials for Ruthenium Complexes and Diquats

	$E_{1/2}$ (V)[a]					
compd	$Ru^{3+/2+}$	$DQ^{2+/+}$	$DQ^{+/0}$	$Ru^{2+/+}$	$Ru^{+/0}$	$Ru^{0/-}$
RuL[a]	0.91			−1.65	−1.86	−2.13
RuL_{DQ}[b]	0.91	−0.90	−1.32	−1.77	−1.92	
$[Ru(bpy)_3]^{2+}$ [b]	0.89			−1.74	−1.93	−2.18
Ru(424-DQ)[c]	0.85	−1.15	−1.28	−1.75	−1.95	−2.21
$4DQ^{2+}$ [d]		−1.02				
Ru(422-DQ),[c]	0.87	−0.82	−1.27	−1.73	−1.94	−2.19
$2DQ^{2+}$ [d]		−0.73	−1.2			
4,4′-dimethyl-$2DQ^{2+}$ [b]		−0.87				

[a] All values measured in CH_3CN and converted to vs Fc^+/Fc using conversion constants in ref 70. [b] Ref 31. [c] Ref 3. [d] Ref 71.

for RuL (Figure 4b). Spectra of the terminal excited states (i.e., C in *Scheme 1*) obtained by adding the scaled ground state absorption spectrum to transient difference spectra are shown by the black curves in Figures 7 and 8c for RuL_{DQ} and RuL, respectively. The long lifetime and emissive character point to a ^{3}MLCT state for RuL, while the nanosecond lifetime and lack of emission suggest a CS state is formed in the case of RuL_{DQ}. We discuss the nature of these long-lived excited states in more detail in the following subsections before analyzing the short-time dynamics in section 4.3.

Feasibility of Intramolecular ET Quenching. Although MLCT states of ruthenium polypyridyl complexes can be thought of as intramolecular ET states in which an electron is transferred from ruthenium to a coordinated ligand, our interest here is in charge-separated states in which an electron is transferred from Ru to a more distant electron acceptor. Bipyridinium compounds, including diquat, efficiently quench the luminescence of photoexcited $[Ru(bpy)_3]^{2+}$.[42,43] Covalently linking these same compounds to a polypyridyl ligand quenches the long-lived emission characteristic of many ruthenium photosensitizers by intramolecular ET from the metal to the bipyridinium acceptor.[4,20,44] The driving force for forward ET, $-\Delta G_{ET}$, can be estimated from the Rehm−Weller equation (eq 5),[45]

$$-\Delta G_{ET} = e[E_{1/2}(A/A^{\bullet -}) - E_{1/2}(D^{\bullet +}/D)] + E_{00} - w(r_{DA}) \quad (5)$$

In this equation, $E_{1/2}$ values are reduction potentials, e is the fundamental charge, E_{00} is the singlet energy of the excited donor or acceptor, w is the "work term" or energy change when the distance between donor and acceptor radical ions is decreased from infinity to the distance r_{DA} at which an electron is transferred from donor D to acceptor A. We neglect w, which is small in a polar solvent like acetonitrile,[6,19,32] and approximate the driving force for forward ET as,

$$-\Delta G_{ET} = e[E_{1/2}(L/L^{\bullet -}) - E_{1/2}(Ru^{3+/2+})] + E_{00} \quad (6)$$

Using reduction potentials from Table 3, $-\Delta G_{ET} = E_{00} - 2.56$ eV for RuL. The value of E_{00} for RuL was approximated by the energy of maximum emission at room temperature (1.84 eV[31]). This value is too small to yield a positive ET driving force, and ET quenching of the ^{3}MLCT state does not take place in photoexcited RuL, consistent with its emissive character and long excited state lifetime that approaches 1 μs.[31]

For RuL_{DQ}, the reduction potential data in Table 3 predicts $-\Delta G_{ET} = E_{00} - 1.81$ eV. Because RuL_{DQ} is nonemissive, E_{00}

was assumed to have the same value of 1.84 eV as RuL. This value yields a slightly favorable driving force for forward ET. The use of the room temperature emission maximum likely underestimates the true value of E_{00}, and the true driving force is likely to be somewhat larger, especially because ET appears to take place faster than relaxation in the initial excited state. Thus, electrochemical considerations suggest that intramolecular ET quenching is feasible for RuL_{DQ}, but not for RuL.

State C in RuL_{DQ} Is a CS State. The transient spectra for RuL_{DQ} show strong positive signals ($\Delta A > 0$) at wavelengths >460 nm with a maximum at 505 nm (Figure 3). These features arise from the L_{DQ} ligand because $[Ru(bpy)_3]^{2+}$ shows only very weak transient absorption at probe wavelengths >500 nm.[46] The transient spectra in the rightmost column in Figure 3 are identical at all delay times after scaling, consistent with the decay of a single species to the ground state. In view of the positive signals, the molar absorption coefficient (ε) of this single transient species must exceed that of the RuL_{DQ} ground state, which we estimate to be 13 300 M^{-1} cm^{-1} at 500 nm, the ^{1}MLCT maximum. The radical cation produced by one electron reduction of $4DQ^{2+}$ (Chart 1) has λ_{max} near 500 nm, but an ε value of only 2 500 M^{-1} cm^{-1}.[47] Furthermore, an intense absorption band is seen for the reduced diquat near 390 nm with a roughly 3-fold larger ε than at 500 nm,[47] but no such band is seen in the spectrum of state C. Both observations indicate that the spectrum of state C of RuL_{DQ} (see Figure 7) bears little resemblance to the much weaker visible wavelength absorption by reduced diquats such as $4DQ^{\cdot+}$ tethered to ruthenium via alkyl linkers.[44]

The extensive π conjugation present in the L_{DQ} ligand can, of course, be expected to strongly perturb the spectrum of the reduced diquat. In fact, the spectrum of state C (Figure 7) with its intense absorption near 500 nm and the spectrum of the radical cation produced by one electron reduction of *trans*-1,2-bis(*N*-methyl-4-pyridiniumyl)ethylene (*trans*-bpe)[48−50] are very similar, suggesting that the excited electron is delocalized over the L ligand, producing a diazastilbene-like radical. The radicals produced by one electron reduction of substituted *trans*-stilbenes absorb intensely at visible wavelengths. For example, *trans*-bpe has λ_{max} of 517 nm and a large ε of 57 000 M^{-1} cm^{-1}.[49] Replacing the terminal methyl groups by benzyl groups yields the "vinylene viologen", 1,2-bis(*N*-benzyl-4-pyridinium)ethylene dibromide, which has essentially the same spectrum as *trans*-bpe.[51]

Insights from Electrochemistry. Electrochemical data support the conclusion that a CS state is formed in RuL_{DQ} and can be used to identify the lowest ^{3}MLCT state of RuL. Table 3 summarizes reduction potential data for RuL, RuL_{DQ} and several related compounds (see structures in Chart 1). For a mixed-ligand complex, the lowest energy ^{3}MLCT transition ($d\pi \rightarrow \pi^*$) is associated with the ligand having the lowest π^* level.[52] For the Ru−diquat complexes Ru(422-DQ) and Ru(424-DQ), which have an alkyl bridge, the most facile reduction waves correspond to reduction of the terminal diquat, and the values differ little from those of the isolated diquats $2DQ^{2+}$ and $4DQ^{2+}$, especially when the electron-releasing effect of the 4-methyl group is taken into account. Comparison of $E_{1/2}(DQ^{2+/+})$ for $2DQ^{2+}$ with $E_{1/2}(DQ^{2+/+})$ for 4,4′-dimethyl-$2DQ^{2+}$ shows that this latter effect results in a cathodic shift of about 140 mV. In contrast, the π-conjugated bridge in RuL_{DQ} causes the first reduction to occur at a significantly more positive voltage. Thus, the first reduction potential of RuL_{DQ} is 0.25 V more positive than that of $(bpy)_2Ru(424\text{-}DQ)$ and 0.12 V more positive than that of $4DQ^{2+}$. The greater ease of reduction of L_{DQ} is due to its greater conjugation length. $E_{1/2}$ for the $DQ^{+/0}$ reduction is similar for RuL_{DQ} and the two alkyl-linked Ru-diquat complexes, Ru(422-DQ) and Ru(424-DQ), which may be because the second reduction potential of diquats is relatively independent of conformation.[53]

The $Ru^{2+/+}$ and $Ru^{+/0}$ potentials are very similar for RuL_{DQ}, Ru(424-DQ), Ru(422-DQ), and $[Ru(bpy)_3]^{2+}$ (Table 3), indicating that these couples describe reductions on bpy ligands. The $Ru^{2+/+}$ potential is usually assumed to correspond to the most facile ligand reduction,[3] but it would be incorrect to conclude that the lowest-energy ^{3}MLCT state of RuL_{DQ} is bpy-based, as in Ru(424-DQ).[3] Unlike the alkyl-tethered bipyridinium ligands such as 424-DQ, delocalization in RuL_{DQ} makes it impossible to separate the electrochemistry taking place on opposite ends of the L_{DQ} ligand. Because of the ethenyl bridge, the first added electron does not localize on diquat but, instead, occupies a lowest-energy π^* molecular orbital that is delocalized across the ligand, inhibiting further reduction of the metal-coordinating end of the ligand. In alkyl-linked compounds, it is reasonable to think of the ruthenium-ligating bipyridine and the electron acceptor as electronically distinct species, but this is no longer the case in the RuL_{DQ} compound, as is already indicated by the strongly red-shifted MLCT band in the absorption spectrum. The broad and intense shape of the lowest-energy absorption band of L_{DQ} is consistent with sizable delocalization of the excited electron,[54] which is possible only on the L_{DQ} ligand. We conclude that the lowest-energy ^{3}MLCT state of RuL_{DQ} is associated with the L_{DQ} ligand.

The difference between the first and second diquat potentials of 0.13 V for Ru(424-DQ) increases to 0.42 V for RuL_{DQ}. This is evidence that the first reduction is particularly facile for RuL_{DQ}, consistent with the lower energy of the electron that is delocalized through the entire π-system of the ligand. The electrochemical data clearly show that the most favorable reduction of the ligand L_{DQ} occurs at a more positive potential than the isolated diquat $4DQ^{2+}$. The electrochemistry thus leads to the conclusion that the state in which the electron is delocalized over the bridge is lower in energy than the state in which it resides on the diquat end of the ligand.

Meyer and co-workers studied the photophysics of ruthenium complexes with our same L ligand, but with ancillary dmb ligands in place of bpy ligands.[18,55] Resonance Raman and other evidence indicated that the lowest ^{3}MLCT state of a dinuclear ruthenium complex bridged by ligand L is delocalized over both bipyridine rings of the L ligand.[18] Changes in vibrational frequencies seen for this complex and for $L^{\bullet-}$ match those seen upon one electron reduction of *trans*-stilbene.[18] Strouse et al. did not obtain resonance Raman spectra for $(dmb)_2RuL$, the mononuclear complex from their study, but electrochemical measurements support assignment of the lowest-energy ^{3}MLCT state of the mononuclear complex to the L ligand. The first ligand-based reduction ($Ru^{2+/+}$) for RuL is 90 mV more positive than the first ligand-based reduction couple for $[Ru(bpy)_3]^{2+}$, showing that the lowest ^{3}MLCT state of RuL is localized on the L ligand. Furthermore, the wavelength of maximum emission for RuL ($\lambda_{max}^{em} = 675$ nm) is considerably red-shifted compared to $[Ru(bpy)_3]^{2+}$ ($\lambda_{max}^{em} = 600$ nm), consistent with a lowest-energy ^{3}MLCT state on the L ligand.

State C for RuL Is a ^{3}MLCT State. As described above, state C of RuL is assigned to a ^{3}MLCT state on the basis of its long lifetime. The electrochemical data just discussed indicate that the lowest energy ^{3}MLCT state of RuL is localized on the L ligand. Consistent with this assignment, state C lacks strong absorption near 370 nm, where bpy^- absorption is the dominant

contribution to excited state absorption by the ^{3}MLCT state of $[Ru(bpy)_3]^{2+}$.[46] In addition, the broad band with λ_{max} of 580 nm observed in the transient difference spectrum for state C is not seen in the spectrum of the bpy-localized ^{3}MLCT state of $[Ru(bpy)_3]^{2+}$.[46]

The ^{3}MLCT spectrum of many ruthenium polypyridyl complexes resembles the reductive difference spectrum of the electron-accepting ligand,[56] but the spectrum of state C of RuL (black curve in Figure 8c) differs markedly from the spectrum of reduced L (Figure 2b). We considered two possible explanations for this observation. The first explanation, originally suggested by Schmehl and co-workers,[57,58] is that both a ligand-localized $^3\pi\pi^*$ state and the lowest energy ^{3}MLCT state of the complex are populated by intersystem crossing from the initial photoexcited state of the complex. If population interconversion between these two triplet states is slow, then both could potentially contribute to our pump−probe signals. In this scenario, the 10-fold smaller quantum yield of emission[31] seen for RuL as compared with $[Ru(bpy)_3]^{2+}$ would be explained by emission that arises solely from the ^{3}MLCT state, which is populated to a smaller degree than the nonemissive, ligand-based $^3\pi\pi^*$ state. Excited state absorption by the latter state could then dominate the transient spectrum instead of the $L^{\bullet-}$-like absorption expected for the ^{3}MLCT state. Furthermore, population of the $^3\pi\pi^*$ state of the ligand could induce cis−trans isomerization[57] consistent with the detection of small amounts of cis isomer by Zhang et al. for RuL in aqueous solution.[31]

A second possible explanation for why the C state spectrum differs from that of $L^{\bullet-}$ is that the electron in the excited RuL complex is not fully delocalized on L, as in the bare, reduced ligand, but is, instead, restricted to the bipyridine closest to ruthenium. The energy of the bridge state may be too high to overcome the electrostatic stabilization that keeps the excited electron close to the metal core. This conclusion is supported by the electrochemical data showing that the most favorable reduction of RuL is 0.75 V less favorable than that of RuL_{DQ}. This explanation appears to contradict the finding of extensive excited-state delocalization in the lowest ^{3}MLCT state of a biruthenium complex bridged by the L ligand by Meyer and co-workers from resonance Raman experiments.[18] However, Schmehl et al. pointed out that the Raman evidence obtained by Meyer and co-workers does not rule out a localized triplet state of the ligand because such a triplet state is expected to have vibrational bands similar to the radical anion of ligand L.[57]

4.3. Short-Time Dynamics and Assignment of States A and B. We next consider what the short-time signals reveal about the precursor states (states A and B in *Scheme 1*) seen in RuL and RuL_{DQ}. The shortest lifetime (τ_1 in Tables 1 and 2) is responsible for the decay in transient absorption at 375 nm and the rapid growth in the bleach signal probed at 450 nm (Figure 5). This behavior is seen for both RuL and RuL_{DQ}, although the signal changes are less pronounced for the former compound. The rapid decay seen at 375 nm is not observed in $[Ru(bpy)_3]^{2+}$ at the nearby probe wavelength of 360 nm,[11] indicating that it is unique to the mixed-ligand complexes. The magnitude of the signal change at 375 nm is too large to be due to thermalization of an excited state or solvation dynamics. Instead, these signals are indicative of population change between electronic states. Two possibilities were considered: internal conversion to the ground state and internal conversion among excited states.

Internal conversion to the ground state, perhaps in response to isomerization about the double bond of the asymmetric ligand, could explain the rapid recovery of the bleach signal at 450 nm (Figure 5b). However, Strouse et al.[18] observed no evidence for photoisomerization in either L-functionalized mono- and dinuclear ruthenium complexes or in the bare ligand L. A very small amount of *cis*-$[(bpy)_2RuL]^{2+}$ was observed in an unirradiated aqueous solution of RuL, and the amount of the cis form increased slightly upon photoirradiation.[33] This could indicate that photoisomerization occurs to a small extent for RuL, but isomerization appears to be strongly disfavored for RuL_{DQ} on steric and electrostatic grounds.[18] In addition, the steady-state absorption spectrum should show changes due to isomerization,[59,60] but no changes to the UV/vis spectra of either RuL or RuL_{DQ} were observed in our experiments in acetonitrile solution after prolonged UV or visible irradiation. We therefore rule out excited state deactivation by isomerization as a significant deactivation pathway. Instead, we assign the signal evolution shown in Figure 5 to decay of excited states localized on the asymmetric ligand and to higher-lying ^{3}MLCT states as discussed separately for RuL_{DQ} and RuL in the following.

RuL_{DQ}. As mentioned earlier, the same final state (state C) is rapidly produced at all excitation wavelengths, despite the rather different initial states prepared by the various pump wavelengths. As is evident in Figure 1, the 320 nm pump pulse excites mainly a ligand-localized $^1\pi\pi^*$ transition associated with the double bond of ligand L_{DQ}. The 600 nm pump pulse excites only the long-wavelength ^{1}MLCT transition associated with the L_{DQ} ligand, whereas excitation at 400 nm excites higher-energy ^{1}MLCT transitions localized on bpy ligands.

During delay times when the τ_2 decay takes place, the transient spectrum observed following excitation at 320 and 400 nm shifts noticeably to shorter wavelengths (see Figures 3b and 3e). This spectral blue shifting is assigned to vibrational cooling of the rapidly formed CS state. Vibrational cooling in acetonitrile typically occurs with a time constant of 10 ps,[61,62] and its observation in RuL_{DQ} provides clear evidence that the reduced ligand is formed more rapidly than excess vibrational energy can be relaxed to the solvent.

The spectrum of species B in Figure 6c and d is red-shifted with respect to the spectrum of the CS state (species C), as expected if the B state is the CS state with excess vibrational energy. Because $k_1 \gg k_2$, k_3 eq 3 for the SADS of state B becomes

$$\mathrm{SADS(B)} \approx \mathrm{DADS}(k_2) + \mathrm{DADS}(k_3) \qquad (7)$$

$\mathrm{DADS}(k_2)$ (green curve in Figure 6a and b) closely resembles the first derivative with respect to wavelength of $\mathrm{DADS}(k_3)$, and eq 7 therefore amounts to summing a function and its first derivative, explaining why SADS(B) and SADS(C) are similar in shape, but displaced from one another along the wavelength axis.

For RuL_{DQ} pumped at 600 nm, only two exponentials are required to fit the observed signals (Table 1). Although the transient spectra between 8 and 80 ps (Figure 3h) fluctuate somewhat randomly in amplitude due to laser noise, there is no longer the systematic blue shift and spectral narrowing that appears on this time scale for excitation at 320 nm (Figure 3b) and 400 nm (Figure 3e). Instead, the spectrum of the CS state is visible at the earliest delay times (Figure 3g). Target analysis was carried out with just two states, A and C, omitting state B in *Scheme 1*. SADS(A) is similar to SADS(C), but is red-shifted. We therefore assign the rapid dynamics ($\tau \approx 0.6$ ps) seen for excitation at 600 nm mainly to vibrational cooling, which occurs more rapidly due to the reduced amount of excess vibrational energy deposited by this longer pump wavelength.

Finally, we discuss the spectra calculated for state A (purple curves in Figure 7), the state that decays with the shortest lifetime (τ_1). It might have been expected that the spectrum seen at earliest times for RuL_{DQ} before ET has taken place would resemble the final spectrum C of RuL, but SAS(A) for RuL_{DQ} bears little resemblance to SAS(C) for RuL (Figure 8c). As discussed above, state C for RuL may be dominated by absorption from the $^3\pi\pi^*$ state of the ligand, a state that is not seen in RuL_{DQ}. Instead, SAS(A) for RuL_{DQ} has two bands on either side of the spectrum of the long-time CS state. We propose that the A spectrum is due chiefly to excited-state absorption by the $^1\pi\pi^*$ state of the L_{DQ} ligand. Excited state absorption by *trans*-bpe in acetonitrile (produced by excitation at 308 nm with a 70 fs pulse) displays a sharp peak near 515 nm.[63]

RuL. ET quenching of the lowest ^{3}MLCT state cannot take place in RuL, and we propose that the τ_1 and τ_2 dynamics reflect the rapid decay of the L-localized $^1\pi\pi^*$ state, decay from higher-energy MLCT states, or both. The spectrum of state A (purple curve, Figure 8c) is similar to the spectrum of state A of RuL_{DQ} (purple curve, Figure 7b), suggesting that it should be assigned to the $^1\pi\pi^*$ state of the L ligand. The SAS(B) spectrum for RuL (green curve, Figure 8c) is similar to the excited-state absorption spectrum of $[Ru(bpy)_3]^{2+}$ (ref 46) and could be due to a higher-energy ^{3}MLCT state localized on one of the bpy ligands. If this is correct, then time constant τ_2 (= 2.6 ps) would measure the time for interligand electron transfer (ILET) to occur to the lowest energy (L-localized) ^{3}MLCT state. As Benniston and Harriman recently commented,[64] substantial uncertainty exists about the time required for ILET, with estimates ranging from <1 ps to hundreds of picoseconds.[9−11,65−67] Liard and Vlček[68] extracted ILET dynamics from magic angle transient absorption signals for the mixed-ligand complex $[Re(MQ^+)(CO)_3(dmb)]^{2+}$, in which MQ^+ is *N*-methyl-4,4′-bipyridinium and dmb is 4,4′-dimethyl-2,2′-bipyridine. They concluded that excitation of this complex at 400 nm produces a mixture of MLCT states associated with the MQ^+ and dmb ligands and is followed by ILET from dmb to MQ^+ in 8.3 ps in acetonitrile.[68] An even faster time constant of 1.5 ps was reported by Shaw et al. for ILET in an osmium mixed-ligand complex, which they attributed to the larger driving force for ET as compared with the symmetric-ligand complex.[10] This estimated ILET time is thus consistent with past estimates for asymmetric complexes.

Alternatively, the weak growth occurring with $\tau_2 = 2.6$ ps near 430 and 580 nm in the transient spectrum of RuL could arise from formation of the $^3\pi\pi^*$ state of ligand L from the ligand-based $^1\pi\pi^*$ state. Excited state absorption by the ligand-localized triplet state of the related ligand 1,4-bis[2-(4′-methyl-2,2′-bipyrid-4-yl)ethenyl]benzene occurs at 445 ± 10 and 500 ± 10 nm in acetonitrile.[69] Further experiments are needed to decide whether the short-time RuL dynamics are due to decay in the manifold of ^{3}MLCT states or to intersystem crossing to a ligand-localized triplet state.

4.4. Comparison with ET Rates in Other Dyads. The RuL_{DQ} experiments show that the CS state is reached with a time constant of no more than ∼1 ps, regardless of the locus of initial excitation ($^1\pi\pi^*$ state of the asymmetric ligand or any of the various ^{1}MLCT states). This shows that excitation of the ligand-localized state of the functionalized ligand does not significantly retard the formation of the CS state. Previously, Damrauer et al. showed that the ^{3}MLCT state of the symmetric complex $[Ru(bpy)_3]^{2+}$ is reached no more than 300 fs after excitation.[7] For excitation at 600 nm, there is no evidence of intermediate ^{3}MLCT absorption, and the pump pulse instead appears to transfer a dπ electron from ruthenium more or less instantaneously ("optical ET") to the delocalized state on the L_{DQ} ligand.

For the shorter pump wavelengths, the CS state appears somewhat more slowly, but nevertheless with a time constant of just 1 ps because of the time needed for decay of the $^1\pi\pi^*$ state associated with the L_{DQ} ligand or decay of higher energy MLCT states. Unfortunately, it is unknown from these measurements whether ET occurs directly from the ligand-localized excited state of L_{DQ} or whether this state must first decay to the lowest-energy ^{3}MLCT state. If it is correct that formation of the CS state proceeds from the lowest-energy ^{3}MLCT state, then our results indicate that both ISC and ILET from higher-lying MLCT states are complete in the asymmetric complex RuL_{DQ} on the subpicosecond time scale.

Forward ET to produce the CS state of RuL_{DQ} occurs at a strikingly high rate compared to other ruthenium-based dyads. Lomoth et al.[6] studied the ruthenium polypyridyl complex formed when methyl viologen connected by a single methylene group to the 4′ position of a ligating 2,2′-bipyridine and reported a time constant of 4.5 ± 0.5 ps for forward ET. Inserting a second methylene group in the bridge slowed the forward ET time constant to 200 ps. The Ru(424-DQ) complex (chart 1) studied by Cooley et al.[3] in which the ethenyl linker is replaced by a saturated bridge consisting of two methylene units exhibits transient absorption bleach recovery and emission decay times of just over 6 ns. Our results show that replacing the ethyl linker by an ethenyl linker dramatically accelerates the rate of ET quenching. The electron may not have to travel as far in RuL_{DQ} because the electron accepting state is delocalized "back onto" the bridge. Delocalization may also reduce the reorganization energy, allowing the rate of forward ET to proceed at the maximal rate for the available driving force.[5]

Not only is the CS state of the RuL_{DQ} complex formed rapidly, but it also undergoes charge recombination more slowly than is observed in nearly all ruthenium−bipyridinium complexes studied to date. The rate of back ET was much faster than the rate of forward ET in all Ru-diquat dyads studied by Cooley et al.[3] Kelly and Rodgers reported faster rates for back ET than for forward ET in Ru−viologen dyads with flexible polymethylene linkers whenever forward ET took place in nanoseconds.[4]

5. Conclusions

Excited-state dynamics of two mixed-ligand ruthenium complexes was investigated by broadband femtosecond transient absorption spectroscopy. In RuL, our results provide evidence for subpicosecond ILET, which rapidly transfers population to the lowest energy ^{3}MLCT state. In RuL_{DQ}, intramolecular charge transfer occurs in ≤1 ps, forming a CS state with the relatively long lifetime of ∼1.4 ns. Forward ET in the dyad may occur competitively with the relaxation of upper excited states. Target analysis provides clear evidence of vibrational cooling by the nascent reduced ligand. It was suggested in an earlier report that photoexcitation of RuL_{DQ} transfers an electron from the metal to the diquat end of the ligand,[31] but the results of this study show instead that the excited electron is delocalized across the π-system of the L_{DQ} ligand. Low energy states associated with π-conjugated bridges could be a general impediment to the robust delivery of an electron to an acceptor in donor−bridge−acceptor compounds. This study also raises the question of the mechanism by which electrons are delivered to further acceptors inside neighboring zeolite cavities.[30] The insights from this study lay the groundwork for investigations on ET dynamics of

ruthenium photosensitizers encapsulated in zeolite cavities, which we will report on soon.

Acknowledgment. Funding from DOE Grant DE-FG02-06ER15776 is gratefully acknowledged.

References and Notes

(1) Wasielewski, M. R. *Chem. Rev.* **1992**, *92*, 435.
(2) Danielson, E.; Elliott, C. M.; Merkert, J. W.; Meyer, T. J. *J. Am. Chem. Soc.* **1987**, *109*, 2519.
(3) Cooley, L. F.; Headford, C. E. L.; Elliott, C. M.; Kelley, D. F. *J. Am. Chem. Soc.* **1988**, *110*, 6673.
(4) Kelly, L. A.; Rodgers, M. A. J. *J. Phys. Chem.* **1995**, *99*, 13132.
(5) Meylemans, H. A.; Lei, C. F.; Damrauer, N. H. *Inorg. Chem.* **2008**, *47*, 4060.
(6) Lomoth, R.; Haupl, T.; Johansson, O.; Hammarstrom, L. *Chem.—Eur. J.* **2002**, *8*, 102.
(7) Damrauer, N. H.; Cerullo, G.; Yeh, A.; Boussie, T. R.; Shank, C. V.; McCusker, J. K. *Science* **1997**, *275*, 54.
(8) Olson, E. J. C.; Hu, D.; Hormann, A.; Jonkman, A. M.; Arkin, M. R.; Stemp, E. D. A.; Barton, J. K.; Barbara, P. F. *J. Am. Chem. Soc.* **1997**, *119*, 11458.
(9) Onfelt, B.; Lincoln, P.; Nordén, B.; Baskin, J. S.; Zewail, A. H. *Proc. Natl. Acad. Sci. U.S.A.* **2000**, *97*, 5708.
(10) Shaw, G. B.; Brown, C. L.; Papanikolas, J. M. *J. Phys. Chem. A* **2002**, *106*, 1483.
(11) Wallin, S.; Davidsson, J.; Modin, J.; Hammarstrom, L. *J. Phys. Chem. A* **2005**, *109*, 4697.
(12) Lainé, P. P.; Bedioui, F.; Loiseau, F.; Chiorboli, C.; Campagna, S. *J. Am. Chem. Soc.* **2006**, *128*, 7510.
(13) Yoon, S.; Kukura, P.; Stuart, C. M.; Mathies, R. A. *Mol. Phys.* **2006**, *104*, 1275.
(14) Cannizzo, A.; van Mourik, F.; Gawelda, W.; Zgrablic, G.; Bressler, C.; Chergui, M. *Angew. Chem., Int. Ed.* **2006**, *45*, 3174.
(15) Henry, W.; Coates, C. G.; Brady, C.; Ronayne, K. L.; Matousek, P.; Towrie, M.; Botchway, S. W.; Parker, A. W.; Vos, J. G.; Browne, W. R.; McGarvey, J. J. *J. Phys. Chem. A* **2008**, *112*, 4537.
(16) McFarland, S. A.; Cheng, K.; Lee, F. S.; Cozens, F. L.; Schepp, N. P. *Can. J. Chem.* **2008**, *86*, 1118.
(17) Aleman, E. A.; Shreiner, C. D.; Rajesh, C. S.; Smith, T.; Garrison, S. A.; Modarelli, D. A. *Dalton Trans.* **2009**, 6562.
(18) Strouse, G. F.; Schoonover, J. R.; Duesing, R.; Boyde, S.; Jones, W. E.; Meyer, T. J. *Inorg. Chem.* **1995**, *34*, 473.
(19) Borgström, M.; Johansson, O.; Lomoth, R.; Baudin, H. B.; Wallin, S.; Sun, L. C.; Åkermark, B.; Hammarström, L. *Inorg. Chem.* **2003**, *42*, 5173.
(20) Yonemoto, E. H.; Riley, R. L.; Kim, Y. I.; Atherton, S. J.; Schmehl, R. H.; Mallouk, T. E. *J. Am. Chem. Soc.* **1992**, *114*, 8081.
(21) Ryu, C. K.; Wang, R. Y.; Schmehl, R. H.; Ferrere, S.; Ludwikow, M.; Merkert, J. W.; Headford, C. E. L.; Elliott, C. M. *J. Am. Chem. Soc.* **1992**, *114*, 430.
(22) Yonemoto, E. H.; Saupe, G. B.; Schmehl, R. H.; Hubig, S. M.; Rilery, R. L.; Iverson, B. L.; Mallouk, T. E. *J. Am. Chem. Soc.* **1994**, *116*, 4786.
(23) Redmore, N. P.; Rubtsov, I. V.; Therien, M. J. *J. Am. Chem. Soc.* **2003**, *125*, 8769.
(24) Monnereau, C.; Gomez, J.; Blart, E.; Odobel, F.; Wallin, S.; Fallberg, A.; Hammarström, L. *Inorg. Chem.* **2005**, *44*, 4806.
(25) Chaignon, F.; Buchet, F.; Blart, E.; Falkenstrom, M.; Hammarstrom, L.; Odobel, F. *New J. Chem.* **2009**, *33*, 408.
(26) Gonzalez-Cabello, A.; Vazquez, P.; Torres, T.; Guldi, D. M. *J. Org. Chem.* **2003**, *68*, 8635.
(27) Coe, B. J.; Harries, J. L.; Helliwell, M.; Brunschwig, B. S.; Harris, J. A.; Asselberghs, I.; Hung, S. T.; Clays, K.; Horton, P. N.; Hursthouse, M. B. *Inorg. Chem.* **2006**, *45*, 1215.
(28) Constable, E. C.; Figgemeier, E.; Housecroft, C. E.; Medlycott, E. A.; Neuburger, M.; Schaffner, S.; Reymann, S. *Polyhedron* **2008**, *27*, 3601.
(29) Ng, Z. Y.; Loh, K. P.; Li, L. Q.; Ho, P.; Bai, P.; Yip, J. H. K. *ACS Nano* **2009**, *3*, 2103.
(30) Kim, Y.; Das, A.; Zhang, H. Y.; Dutta, P. K. *J. Phys. Chem. B* **2005**, *109*, 6929.
(31) Zhang, H. Y.; Rajesh, C. S.; Dutta, P. K. *J. Phys. Chem. C* **2009**, *113*, 4623.
(32) Johansson, O.; Borgstrom, M.; Lomoth, R.; Palmblad, M.; Bergquist, J.; Hammarstrom, L.; Sun, L. C.; Akermark, B. *Inorg. Chem.* **2003**, *42*, 2908.
(33) Zhang, H.; Rajesh, C. S.; Dutta, P. K. *J. Phys. Chem. A* **2008**, *112*, 808.
(34) Burdzinski, G.; Hackett, J. C.; Wang, J.; Gustafson, T. L.; Hadad, C. M.; Platz, M. S. *J. Am. Chem. Soc.* **2006**, *128*, 13402.
(35) van Stokkum, I. H. M.; Larsen, D. S.; van Grondelle, R. *Biochim. Biophys. Acta: Bioenerg.* **2004**, *1657*, 82.
(36) Beechem, J. M.; Ameloot, M.; Brand, L. *Anal. Instrum.* **1985**, *14*, 379.
(37) Juris, A.; Balzani, V.; Barigelletti, F.; Campagna, S.; Belser, P.; Vonzelewsky, A. *Coord. Chem. Rev.* **1988**, *84*, 85.
(38) Zhou, Q. X.; Lei, W. H.; Li, C.; Hou, Y. J.; Wang, X. S.; Zhang, B. W. *New J. Chem.* **2010**, *34*, 137.
(39) Benniston, A. C.; Harriman, A.; Grosshenny, V.; Ziessel, R. *New J. Chem.* **1997**, *21*, 405.
(40) Hayes, M. A.; Meckel, C.; Schatz, E.; Ward, M. D. *J. Chem. Soc., Dalton Trans.* **1992**, 703.
(41) Kim, Y.; Lee, H.; Dutta, P. K.; Das, A. *Inorg. Chem.* **2003**, *42*, 4215.
(42) Amouyal, E.; Zidler, B.; Keller, P.; Moradpour, A. *Chem. Phys. Lett.* **1980**, *74*, 314.
(43) Kalyanasundaram, K. *Coord. Chem. Rev.* **1982**, *46*, 159.
(44) Elliott, C. M.; Freitag, R. A.; Blaney, D. D. *J. Am. Chem. Soc.* **1985**, *107*, 4647.
(45) Rehm, D.; Weller, A. *Isr. J. Chem.* **1970**, *8*, 259.
(46) Yoshimura, A.; Hoffman, M. Z.; Sun, H. *J. Photochem. Photobiol. A: Chem.* **1993**, *70*, 29.
(47) Tsukahara, K.; Wilkins, R. G. *J. Am. Chem. Soc.* **1985**, *107*, 2632.
(48) Happ, J. W.; Whitten, D. G.; Ferguson, J. A. *J. Org. Chem.* **1972**, *37*, 1485.
(49) Ebbesen, T. W.; Akaba, R.; Tokumaru, K.; Washio, M.; Tagawa, S.; Tabata, Y. *J. Am. Chem. Soc.* **1988**, *110*, 2147.
(50) Muramatsu, T.; Toyota, A.; Ikegami, Y. *J. Org. Chem.* **1995**, *60*, 4925.
(51) Nanasawa, M.; Miwa, M.; Hirai, M.; Kuwabara, T. *J. Org. Chem.* **2000**, *65*, 593.
(52) McClanahan, S. F.; Dallinger, R. F.; Holler, F. J.; Kincaid, J. R. *J. Am. Chem. Soc.* **1985**, *107*, 4853.
(53) Thummel, R. P.; Lefoulon, F.; Chirayil, S.; Goulle, V. *J. Org. Chem.* **1988**, *53*, 4745.
(54) Hammarstrom, L.; Barigelletti, F.; Flamigni, L.; Indelli, M. T.; Armaroli, N.; Calogero, G.; Guardigli, M.; Sour, A.; Collin, J. P.; Sauvage, J. P. *J. Phys. Chem. A* **1997**, *101*, 9061.
(55) Boyde, S.; Strouse, G. F.; Jones, W. E.; Meyer, T. J. *J. Am. Chem. Soc.* **1990**, *112*, 7395.
(56) Curtright, A. E.; McCusker, J. K. *J. Phys. Chem. A* **1999**, *103*, 7032.
(57) Baba, A. I.; Shaw, J. R.; Simon, J. A.; Thummel, R. P.; Schmehl, R. H. *Coord. Chem. Rev.* **1998**, *171*, 43.
(58) Wang, X. Y.; Del Guerzo, A.; Schmehl, R. H. *J. Photochem. Photobiol., C* **2004**, *5*, 55.
(59) Yutaka, T.; Mori, I.; Kurihara, M.; Mizutani, J.; Kubo, K.; Furusho, S.; Matsumura, K.; Tamai, N.; Nishihara, H. *Inorg. Chem.* **2001**, *40*, 4986.
(60) Zarnegar, P. P.; Bock, C. R.; Whitten, D. G. *J. Am. Chem. Soc.* **1973**, *95*, 4367.
(61) Kovalenko, S. A.; Schanz, R.; Hennig, H.; Ernsting, N. P. *J. Chem. Phys.* **2001**, *115*, 3256.
(62) Middleton, C. T.; Cohen, B.; Kohler, B. *J. Phys. Chem. A* **2007**, *111*, 10460.
(63) Ushakov, E. N.; Nadtochenko, V. A.; Gromov, S. P.; Vedernikov, A. I.; Lobova, N. A.; Alfimov, M. V.; Gostev, F. E.; Petrukhin, A. N.; Sarkisov, O. M. *Chem. Phys.* **2004**, *298*, 251.
(64) Benniston, A. C.; Harriman, A. *Coord. Chem. Rev.* **2008**, *252*, 2528.
(65) Cooley, L. F.; Bergquist, P.; Kelley, D. F. *J. Am. Chem. Soc.* **1990**, *112*, 2612.
(66) Cushing, J. P.; Butoi, C.; Kelley, D. F. *J. Phys. Chem. A* **1997**, *101*, 7222.
(67) Benko, G.; Kallioinen, J.; Myllyperkio, P.; Trif, F.; Korppi-Tommola, J. E. I.; Yartsev, A. P.; Sundstrom, V. *J. Phys. Chem. B* **2004**, *108*, 2862.
(68) Liard, D. J.; Vlček, A. *Inorg. Chem.* **2000**, *39*, 485.
(69) Shaw, J. R.; Webb, R. T.; Schmehl, R. H. *J. Am. Chem. Soc.* **1990**, *112*, 1117.
(70) Pavlishchuk, V. V.; Addison, A. W. *Inorg. Chim. Acta* **2000**, *298*, 97.
(71) Homer, R. F.; Tomlinson, T. E. *J. Chem. Soc.* **1960**, 2498.

JP102776R